



Shear-induced heat transport and the relevance of generalized Fourier's law in granular Poiseuille flow

Meheboob Alam ^{*}, Ronak Gupta, and Shashank Ravichandir

Engineering Mechanics Unit, Jawaharlal Nehru Centre for Advanced Scientific Research, Bangalore 560064, India

 (Received 11 February 2021; accepted 25 October 2021; published 10 November 2021)

It is shown that both normal and tangential heat-flux profiles in acceleration-driven Poiseuille flow of a granular gas can be qualitatively different from those in a molecular gas. Comparisons with a generalized Fourier's law confirm that the cross-thermal conductivity is responsible for the double-well-shaped profile of the tangential heat flux, and the net heat-flow rate can be directed along or against the external acceleration, depending on the value of the restitution coefficient and the Knudsen number (Kn). Collectively, the tensorial thermal conductivity and the inelasticity-induced clustering of particles can explain the anomalous behavior of shear-induced heat fluxes in a nonrarefied ($Kn \rightarrow 0$) granular gas. The importance of the heat-flux terms driven by the density gradient and the kinetic-stress gradient is discussed in the context of both molecular and granular gases.

DOI: [10.1103/PhysRevFluids.6.114303](https://doi.org/10.1103/PhysRevFluids.6.114303)

I. INTRODUCTION

The plane Poiseuille flow of molecular gases, confined between two “isothermal” walls and driven by a constant body force, or a pressure gradient, served as a prototype to understand various noncontinuum effects (e.g., temperature and velocity slip, thermal creep, Knudsen paradox, temperature bimodality, tangential heat flux, etc.), with seminal works of Maxwell [1], Knudsen [2], Burnett [3], and others [4–10] that spans over a century; the related noncontinuum effects and heat transport are currently being pursued to understand thermo-hydrodynamics of electron flows in graphene [11]. This prototypical flow [see Fig. 1(a) for a schematic] is characterized by inhomogeneous hydrodynamic fields with unidirectional velocity $\mathbf{u} \equiv [u_x(y), 0, 0]$, temperature $T(y)$, and density $\rho(y)$, where x and y denote the flow and transverse or wall-normal directions, respectively. The analogous system of fluidized inelastic grains [12–15] flowing under the action of gravity in a channel is called “granular” Poiseuille flow (GPF) for which the hydrodynamics and rheology were probed recently via simulations [16–18] and theory [19,20], confirming the nontrivial roles of inelastic dissipation and wall conditions (thermal or athermal walls) on (i) the Knudsen paradox [2,11,16], (ii) the bimodal shape [6,7,16,19] of the temperature profile and (iii) the shear viscosity and the normal-stress differences [17,19]. The related flow-induced heat transport phenomenon has not received much attention, except the kinetic theory analysis [19,20] of a “heated” granular gas flowing under gravitational acceleration in a channel. For the latter case, the dependence of the temperature bimodality, viscosity, and normal-stress differences on the restitution coefficient was found to be nonmonotonic [19,20], in contrast to their monotonic dependence in “unheated” GPF [16,17]. The underlying differences have been attributed to the stochastic bulk heating (due to Gaussian white noise) that renders the heated granular gas [19,20] to stay in a state of nearly uniform density at any value of the restitution coefficient unlike in its unheated counterpart

^{*}meheboob@jncasr.ac.in

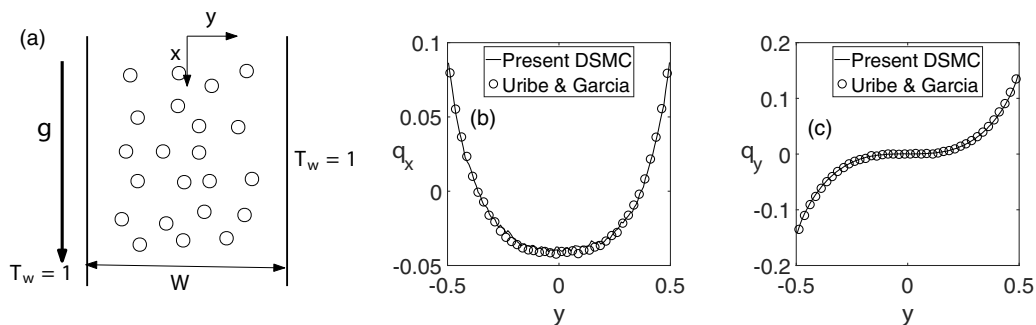


FIG. 1. (a) Schematic of the Poiseuille flow in a channel of width W , bounded by two isothermal walls at $T = T_w$; the flow is driven by gravitational acceleration g along the x direction and the wall-normal coordinate is denoted by y ; see the Supplemental Material [33] for other details. [(b) and (c)] Transverse profiles of (b) tangential heat flux $q_x(y)$ and (c) normal heat flux $q_y(y)$ in a molecular gas undergoing Poiseuille flow: $\text{Kn} = 0.1$ and $\hat{g} = 0.3$. The circles represent the DSMC data of Ref. [8] and the lines denote the present data.

in which the density gradient across the wall-normal direction increases with increasing collisional dissipation [16,17]. The latter effect is likely to bring in certain non-Fourier contributions to heat flux, for example, a Dufour flux term ($\propto \nabla \rho$), the importance of which will be demonstrated here.

In this work we report the role of collisional dissipation on heat transport in GPF via simulations and contrast its behavior with that in a molecular gas. The dissipation-induced signatures of heat fluxes are explained by considering nonlinear effects resulting in a generalized Fourier law, with the latter having relevance in diverse fields encompassing inhomogeneous fluids under extreme deformation [21,22], rarefied gases [3,6,10,23], granular gases [19,24,25], polymeric fluids [26,27], and relativistic fluids [28].

For the canonical problem of the gravity-driven Poiseuille flow [see Fig. 1(a) and the related analysis in Appendix], a simple way to demonstrate the importance of nonlinear effects is to rationalize the appearance of finite streamwise heat flux ($q_x \neq 0$), see Fig. 1(b). In the absence of any temperature gradient along the flow direction ($dT/dx = 0$), the Fourier’s law of heat conduction asserts that $q_x = 0$. Let us consider a tensorial description of the heat-flux vector [21,22,24],

$$\mathbf{q} = -\boldsymbol{\kappa} \cdot \nabla T, \quad (1)$$

with $\boldsymbol{\kappa} = [\kappa_{\alpha\beta}]$ being the (second-rank) thermal conductivity tensor that reduces to an isotropic tensor $\boldsymbol{\kappa} = \kappa \delta_{ij}$, yielding the well-known Fourier’s law of heat conduction $\mathbf{q} = -\boldsymbol{\kappa} \nabla T$, that holds at Navier-Stokes (NS) order. For unidirectional flows, there can be only two nonzero components of $\mathbf{q} \equiv (q_x, q_y, 0)$ given by:

$$q_x = -\kappa_{xy} \frac{dT}{dy} \quad \text{and} \quad q_y = -\kappa_{yy} \frac{dT}{dy}. \quad (2)$$

Therefore a nonzero value of q_x [such as in Fig. 1(b)] is tied to nonzero values of the “cross” thermal conductivity coefficient $\kappa_{xy} \neq 0$. The latter transport coefficient scales like $\kappa_{xy} \propto \sigma_{xy} \propto \dot{\gamma}(y)$ [3,24,29], where σ_{xy} is the shear stress and $\dot{\gamma}(y) = du_x/dy$ is the local shear rate. Since the cross thermal-conductivity scales as $\sigma_{xy} \propto \dot{\gamma}$, the tangential heat flux $q_x = O[\dot{\gamma} \times (dT/dy)]$ is a Burnett order (i.e., second order in the gradients of hydrodynamic fields) effect. Although q_x vanishes at Navier-Stokes (NS) order $O(\dot{\gamma})$, we need to incorporate Burnett-order terms to correctly model the heat-flux variations in a rarefied gas undergoing Poiseuille flow.

Equation (2b) asserts that the origin of the normal heat flux $q_y(y)$ across two isothermal walls in a gravity-driven Poiseuille flow is the shear-induced temperature gradient (dT/dy). In general, the shear-induced heat transport in a rarefied gas, Eqs. (1) and (2), is anisotropic in nature, and deciphering the role of inelasticity on it is the primary focus of the present paper. Note that the

“rarefaction” of a molecular gas is characterized in terms of the Knudsen number ($\text{Kn} = \lambda/W$). However, the underlying classification is rather empirical [30,31]: (i) continuum flow ($\text{Kn} \leq 0.001$) that can be described by NS equations with “no-slip” boundary conditions, (ii) slip flow ($0.01 < \text{Kn} \leq 0.1$) that can be modelled by NS equations with “slip” boundary conditions, (iii) transition flow ($0.1 < \text{Kn} < 10$) and (iv) free molecular flow ($\text{Kn} \geq 10$). Collectively, the slip-flow and transition-flow regimes are called “rarefied” flows for which the extended hydrodynamic equations are recommended. Our work demonstrates that the above classification or suggestion does not strictly hold in a granular or dissipative gas; in particular, we raise questions about the validity of the standard Fourier’s law in the continuum limit ($\text{Kn} \rightarrow 0$) of a granular gas.

With a brief description of the simulation method in Sec. II, the results on heat fluxes in GPF are contrasted with those in a molecular gas in Sec. III. The anomalous shape of the tangential heat flux is explained in Sec. IV, using two variants of Eq. (1) that also incorporates (i) the Dufour flux and (ii) the stress-driven heat flux.

II. SIMULATION METHOD

The inelastic Boltzmann equation is solved by employing the “direct simulation Monte Carlo” (DSMC [31,32]) method, the details of which can be found in the Supplemental Material [33]. The *global* Knudsen number, a measure of the degree of rarefaction of the gas, is defined as $\text{Kn} = \lambda/W$, where W is the channel width and $\lambda = (\sqrt{2}\pi n d^2)^{-1}$ is the equilibrium mean free path of the system at an average number density $n = n_{\text{av}}$. The dimensionless acceleration, defined as

$$\widehat{g} = \frac{gW}{2k_B T_w/m}, \quad (3)$$

quantifies the strength of the body force acting on a particle traveling a distance W ; for example, \widehat{g} is a measure of the strength of the body force between two successive collisions of particles at $\text{Kn} \sim O(1)$ (i.e., when the mean free path is comparable to the channel width $W \sim \lambda$). The dimensionless acceleration is set to $\widehat{g} = 0.5$ in most simulations, and the width of the channel is fixed at $W/d = 1860$ and the Knudsen number,

$$\text{Kn} = (\sqrt{2}\pi n_{\text{av}}^*)^{-1}/(W/d) \in (0.025, 10), \quad (4)$$

is changed by varying the average reduced density $n_{\text{av}}^* = n_{\text{av}} d^3$ over a range of $10^{-5} < n_{\text{av}}^* < 10^{-3}$ that represents a “dilute” gas. The main control parameter to characterize a granular gas is the normal restitution coefficient $e_n \in (0, 1)$, with $e_n = 1$ denoting the case of a molecular gas. In the following, the density is normalized by the average density $\rho_R = \rho_{\text{av}} = m n_{\text{av}}$, the temperature by its wall temperature $T_R = T_w$ and the velocity by $u_R = \sqrt{2k_B T_w/m}$. Without loss of generality, we set the particle mass ($m = 1$), particle diameter ($d = 1$), Boltzmann constant ($k_B = 1$) and wall temperature ($T_w = 1$) to unity.

III. RESULTS AND DISCUSSION

The heat flux is calculated from

$$\mathbf{q}_\alpha(y) = \frac{m}{2} \langle (\mathbf{v}_\alpha - \mathbf{u}_\alpha) |\mathbf{v} - \mathbf{u}|^2 \rangle \equiv (q_x, q_y, 0), \quad (5)$$

where \mathbf{v}_α is the instantaneous particle velocity and $\mathbf{u}_\alpha = \langle \mathbf{v}_\alpha \rangle$ is the coarse-grained or hydrodynamic velocity. The present calculations of (b) tangential (q_x) and (c) normal (q_y) components of the heat flux are validated in Fig. 1, with excellent agreement with previous DSMC data [8] for a molecular gas ($e_n = 1$); note that $\mathbf{q}_\alpha(y)$ is made dimensionless by $q_R = \rho_{\text{av}} u_R^3/2$, with u_R being the reference velocity. As explained in Eq. (2), the nonzero values of q_x and q_y in Fig. 1 are tied to nonequilibrium shearing effects: while the normal heat flux q_y originates from shear-induced temperature gradients that appear at the NS-order $O(\dot{\gamma})$, the origin of q_x is tied to rarefaction effects that appear at the Burnett-order $O(\dot{\gamma}^2)$ [3,4].

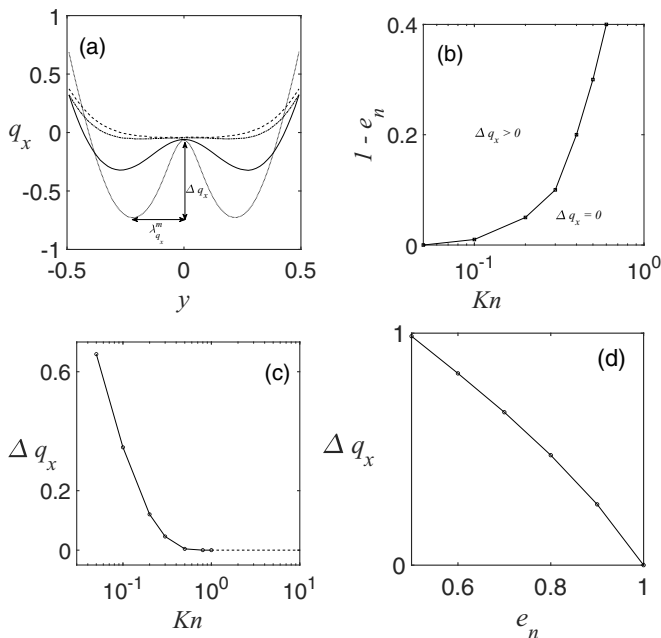


FIG. 2. (a) Effect of restitution coefficient on the tangential heat flux q_x for $Kn = 0.05$: $e_n = 1$ (dashed line), $e_n = 0.99$ (dot-dashed line), $e_n = 0.9$ (solid line), and $e_n = 0.7$ (thin dotted line). (b) Phase diagram in the $(Kn, 1 - e_n)$ plane delineating regions of “double-well” shape q_x (i.e., $\Delta q_x > 0$) and “unimodal” shape q_x (i.e., $\Delta q_x = 0$). [(c) and (d)] Variations of Δq_x with (c) Kn at $e_n = 0.7$ and (d) e_n at $Kn = 0.05$. For all cases, $\hat{g} = 0.5$.

The effect of restitution coefficient ($e_n < 1$) on the tangential heat flux $q_x(y)$ is shown in Fig. 2(a) for $Kn = 0.05$ and $\hat{g} = 0.5$, with the dashed line representing the case of a molecular gas ($e_n = 1$). The corresponding profiles at $Kn = 1$ (i.e., in a rarefied granular gas) look similar to those in Fig. 1(b), with a minimum in $q_x(y)$ at the channel centerline ($y = 0$), representing a molecular gas. Interestingly, in the near-continuum limit ($Kn \sim 0$), a “double-well”-shaped q_x profile emerges in a granular gas, with a local minimum at $y = 0$ and two-symmetric global minima at $y = \pm \lambda_{q_x}^m$ (see the lower-most dotted curve for $e_n = 0.7$), in contrast to its “unimodal” shape in a molecular gas, with $q_x^{\min} = q_x(0)$ and its maxima being located at two walls (the dashed line for $e_n = 1$). We define the relative depth of the double well with respect to its centerline value,

$$\Delta q_x \equiv q_x(0) - q_x^{\min}, \quad \text{at } y = \pm \lambda_{q_x}^m, \quad (6)$$

as marked in Fig. 2(a).

The phase diagram in Fig. 2(b) demarcates the boundary between $\Delta q_x > 0$ (double well) and $\Delta q_x = 0$ (single well) in the $(Kn, 1 - e_n)$ plane. It is clear that the double-well-shaped $q_x(y)$ profile is a small- Kn phenomenon that occurs at any $e_n \neq 1$. Figures 2(c) and 2(d) display the variations of Δq_x with Kn and e_n , respectively. While the increased rarefaction [$Kn > 0.1$ in Fig. 2(c)] diminishes Δq_x , making the q_x profiles of unimodal shape at large-enough values of Kn , the inelastic dissipation [$\propto (1 - e_n^2)$] increases Δq_x in Fig. 2(d). Therefore, the genesis of the double-well-shaped q_x profiles [such as in Fig. 2(a)] is tied to inelastic dissipation, and there is a threshold value of $Kn = Kn_c$, depending on e_n , above which rarefaction dominates over inelastic dissipation, resulting in the well-known unimodal-shaped q_x profiles [viz. Fig. 1(b)] in a molecular gas.

Figures 1(b) and 2(a) indicate that the tangential heat flux around the channel center is directed opposite to the gravitational acceleration (i.e., $q_x < 0$), while it is directed vertically downward

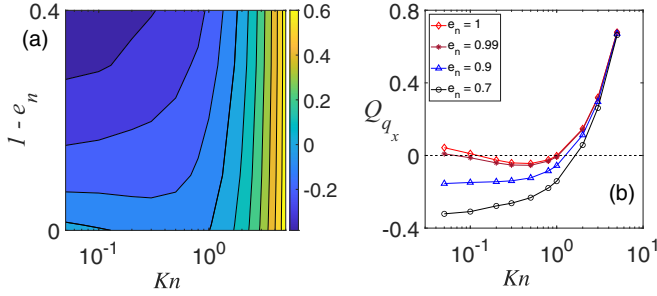


FIG. 3. (a) Phase diagram of the heat-flow rate \mathcal{Q}_{q_x} , Eq. (7), in the $(Kn, 1 - e_n)$ plane; the thick black contour demarcates the regions of positive and negative \mathcal{Q}_{q_x} . (b) Variations of \mathcal{Q}_{q_x} with Kn for different restitution coefficients: $e_n = 1.0$ (red diamonds), 0.99 (brown stars), 0.9 (blue triangles), and 0.7 (black circles). For all cases, $\hat{g} = 0.5$.

($q_x > 0$) near the walls for both molecular ($e_n = 1$) and granular gases. A global measure of q_x can be estimated via

$$\mathcal{Q}_{q_x} = \int_{-1/2}^{1/2} q_x(y) dy, \quad (7)$$

called the ‘‘heat-flow rate’’ [9]. Note that $\mathcal{Q}_{q_x} = 0$ at Navier-Stokes order [$O(\hat{\gamma})$, or, $Kn \rightarrow 0$]; the more rarefied the flow is ($Kn \uparrow$), the larger is the nonequilibrium effect and hence a larger net tangential heat flux.

Figure 3(a) displays the color map of \mathcal{Q}_{q_x} , Eq. (7), in the $(Kn, 1 - e_n)$ plane; the thick black contour marks the loci of $\mathcal{Q}_{q_x} = 0$, to the left and right of which \mathcal{Q}_{q_x} is negative and positive, respectively. Note that the positive or negative values of \mathcal{Q}_{q_x} indicate the direction of the net tangential heat flow along or against the gravitational acceleration. The effect of inelasticity on \mathcal{Q}_{q_x} is quantified in Fig. 3(b), which confirms that the magnitude of \mathcal{Q}_{q_x} increases with decreasing e_n at $Kn \rightarrow 0$. The latter behavior is in stark contrast to the well-known result of $\mathcal{Q}_{q_x} \rightarrow 0$ at $Kn \rightarrow 0$ (for $\hat{g} \rightarrow 0$) in a molecular gas. On the other hand, the variation of \mathcal{Q}_{q_x} at $Kn \rightarrow \infty$ mirrors that in a molecular gas due to the insignificant amount of particle collisions at large values of $Kn > 5$ where the rarefaction is solely responsible for the overall behavior of \mathcal{Q}_{q_x} which is directed along the flow direction (irrespective of the value of the restitution coefficient).

Moving onto the normal heat flux, Figs. 4(a) and 4(b) illustrate the effect of e_n on $q_y(y)$ at (a) $Kn = 0.05$ and (b) $Kn = 1$, with the dashed curve in each panel representing the case of a molecular gas ($e_n = 1$). For both values of Kn , the q_y profiles for $e_n < 1$ differ qualitatively from those in a molecular gas. In particular, for the case of $Kn = 0.05$ [Fig. 4(a)], while $q_y(y > 0) > 0$ and $q_y(y < 0) < 0$ in a molecular gas, even a tiny amount of dissipation ($e_n = 0.99$, marked by dot-dashed line) makes the heat flux to be of the opposite sign compared to that in a molecular gas ($e_n = 1$) over a range of the channel width $-\lambda_{q_y}^m < y < \lambda_{q_y}^m$. These overall observations hold also in the rarefied regime (at $Kn = 1$) if the inelastic dissipation is sufficiently large as confirmed in Fig. 4(b).

The differences in q_y profiles between molecular and granular gases can be quantified in terms of two parameters: (i) the height of the local maxima or minima in $q_y(y)$,

$$\Delta q_y \equiv q_y^{\max} - q_y(0) = q_y(0) - q_y^{\min}, \quad (8)$$

and (ii) the distance of this local extrema from the channel centerline, $y = \pm \lambda_{q_y}^m$, as marked in Fig. 4(a). Figures 4(c) and 4(d) display the variations of (c) Δq_y and (d) $\lambda_{q_y}^m$ with Knudsen number at $e_n = 0.9$ and 0.7 . It is seen that increasing Kn reduces Δq_y at any $e_n \neq 1$ and the inelastic dissipation magnifies its magnitude at any Kn ; both Δq_y and $\lambda_{q_y}^m$ approach zero at large-enough values of $Kn >$

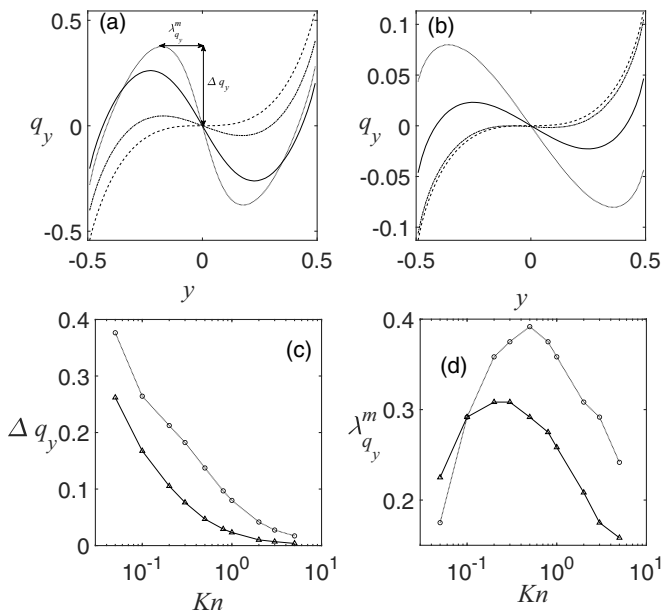


FIG. 4. [(a) and (b)] Effect of restitution coefficient on normal heat flux profiles $q_y(y)$ at (a) $Kn = 0.05$ and (b) $Kn = 1$; $e_n = 1$ (dashed line), $e_n = 0.99$ (dot-dash line), $e_n = 0.9$ (solid line) and $e_n = 0.7$ (thin dotted line). [(c) and (d)] Variations of (c) Δq_y [marked in panel (a)] and (d) $\lambda_{q_y}^m$ with Kn for $e_n = 0.9$ (triangles) and $e_n = 0.7$ (circles). For all cases, $\hat{g} = 0.5$.

1. Therefore, we conclude that the nonmonotonic characteristics of q_y profiles are solely driven by inelasticity and the rarefaction helps in reducing the magnitude of Δq_y . The contrasting shapes of q_y profiles between $e_n = 1$ and $e_n < 1$ in Fig. 4(a) can be explained from the standard Fourier's law if we analyze the corresponding temperature profiles in Fig. 5(a). It is seen that $T(y)$ at $e_n = 0.9$ (dotted line) is of “bimodal” shape, with a temperature minimum at the channel center ($y = 0$) and two local maxima near the walls. Therefore, the positive and negative values of dT/dy [see Fig. 5(b)] on the right and left sides of the channel centerline yield negative and positive values of $q_y(y) \propto -dT/dy$, respectively, resulting in asymmetric q_y profiles in Figs. 4(a) and 4(b).

The origin of the bimodal shape of $T(y)$ in a granular gas [Fig. 5(a)] is tied to the clustering of particles [13,15–17] near the low-shear region around the channel centerline, leading to strongly inhomogeneous density profiles, see Figs. 5(c) and 5(d). Hence, the dissipation-induced temperature bimodality in GPF is responsible for the contrasting q_y profiles between molecular and granular gases in the “nonrarefied” regime [$Kn \rightarrow 0$, Fig. 4(a)]. In the rarefied regime ([$Kn = 1$, Fig. 4(b)], however, a related effect of the rarefaction-driven temperature bimodality [6,20] takes over with increasing Kn , resulting in “anomalous” heat transfer from a colder region to a hotter region as explained in Ref. [33].

The present results on both tangential [Fig. 2(a)] and normal [Fig. 3(a)] heat fluxes in a granular gas ($e_n \neq 1$) are qualitatively different from the theoretical predictions of Ref. [19,20] which can be tied to an ansatz in the theory. In particular, the Boltzmann equation was augmented by adding a white noise term that thermalizes the inelastic particles and the strength of this noise is chosen to compensate for the collisional dissipation; this yields a state of uniform density and temperature (called a heated granular gas, with the adjective “heated” referring to the fact that the energy is continuously fed by stochastic heating of particles) about which a perturbation expansion was sought in terms of a small parameter proportional to the acceleration (i.e., a Froude number or Knudsen number [20]). It was demonstrated that the transverse profiles of $q_x(y)$ (viz. Fig. 10(a)

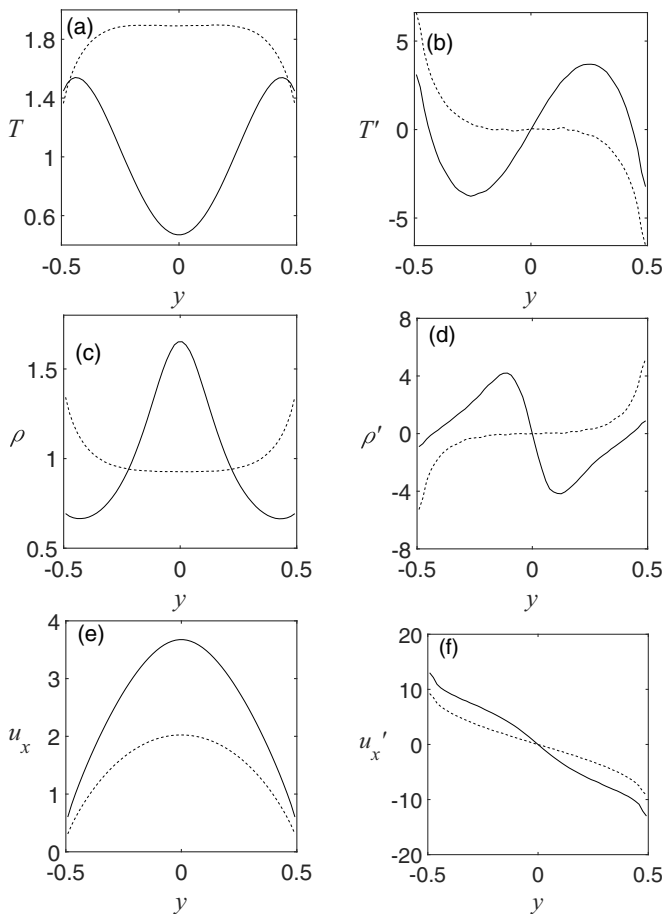


FIG. 5. Transverse profiles of (a) temperature $T(y)/T_w$, (b) temperature gradient $T' = dT/dy \equiv (W/d)dT/d\tilde{y}$, (c) density $\rho(y)/\rho_{av}$, (d) density gradient $\rho' = d\rho/dy \equiv (W/d)d\rho/d\tilde{y}$, (e) streamwise velocity $u_x(y)/u_R$ and (f) velocity gradient $u'_x = du_x/dy \equiv (W/d)du_x/d\tilde{y}$ for $e_n = 1$ (dashed line) and $e_n = 0.9$ (solid line), where $\tilde{y} = y/d$. For all cases, the Knudsen number is $\text{Kn} = 0.05$ and the dimensionless acceleration is $\hat{g} = 0.5$.

and Eq. (80) in Ref. [20]) and $q_y(y)$ (viz. Fig. 11(a) and Eq. (81) in Ref. [20]) in a heated granular gas are of similar shape to those in a molecular gas ($e_n = 1$). Indeed, such bulk stochastic forcing maintains the density field in a nearly homogeneous state at any value of e_n in the limit of small Kn ; other hydrodynamic fields and transport coefficients also behave in a similar manner to those in a molecular gas. A theory, that does not make *a priori* assumptions on the hydrodynamic state of the granular gas, is therefore needed for the present unheated granular gas undergoing Poiseuille flow.

IV. GENERALIZED FOURIER'S LAW FOR A GRANULAR GAS AND ITS PREDICTIONS

To explain the results on (i) the double-well-shaped $q_x(y)$ profiles [Fig. 2(a)] and (ii) the sign of the tangential heat-flow rate Q_x (Fig. 3), we consider an extended version [24,25] of the generalized Fourier's law, Eq. (1),

$$\mathbf{q} = -\kappa^T \cdot \nabla T - \kappa^\rho \cdot \nabla \rho, \quad (9)$$

where κ^T and κ^ρ are the thermal and Dufour conductivity tensors, respectively. For the unidirectional Poiseuille flow, the tangential heat flux follows from Eq. (9):

$$q_x = -\kappa_{xy}^T \frac{dT}{dy} - \kappa_{xy}^\rho \frac{d\rho}{dy} \equiv q_x^T + q_x^\rho, \quad (10)$$

that contains only the ‘‘cross’’ thermal- and Dufour-conductivity coefficients ($\kappa_{xy}^T, \kappa_{xy}^\rho$).

A. Extended hydrodynamic theory of Reddy and Alam (2020)

The expressions for ($\kappa_{xy}^T, \kappa_{xy}^\rho$) are taken from the recent theory of Reddy and Alam [29] who derived ‘‘regularized’’ constitutive relations for a rarefied granular gas. This theory is based on the Grad-moment expansion [4] of the nonequilibrium distribution function, in terms of Hermite polynomials, around the rest state, resulting in three sets of constitutive relations for (i) 14, (ii) 13, and (iii) 10 hydrodynamic-like field variables. Considering their regularized 10-moment theory [29] and retaining terms that are second order in the gradients of hydrodynamic fields, the explicit expressions for the cross-conductivity coefficients are given as

$$\kappa_{xy}^T = \frac{5}{2} \frac{\tau_r}{\alpha(e_n)} \sigma_{xy} \equiv -c_x^T \left(\frac{1}{\rho d^4} \frac{du_x}{dy} \right) \quad \text{and} \quad \kappa_{xy}^\rho = -\frac{T}{\rho} \frac{\tau_r}{\alpha(e_n)} \sigma_{xy} \equiv c_x^\rho \left(\frac{T}{\rho^2 d^4} \frac{du_x}{dy} \right), \quad (11)$$

where $\tau_r = 1/(nd^2\sqrt{\pi T/m})$ is the relaxation time, $\alpha(e_n) = (1 + e_n)(49 - 33e_n)/15$ and $\sigma_{xy} = -2\mu(du_x/dy)$ is the shear stress, with $\mu = 5\sqrt{T}/[4d^2\sqrt{\pi m}(1 + e_n)(3 - e_n)]$ being the shear viscosity of a dilute granular gas. In the final expressions in Eq. (11), two constants (c_x^T, c_x^ρ) are given by

$$c_x^T = \frac{375}{4\pi(1 + e_n)^2(3 - e_n)(49 - 33e_n)} \quad \text{and} \quad c_x^\rho = \frac{2}{5} c_x^T. \quad (12)$$

It is clear from Eq. (11) that both transport coefficients ($\kappa_{xy}^T, \kappa_{xy}^\rho$) are driven by the shear stress, thus tying their origin to ‘‘shear-induced’’ heat transport. Note further that the Dufour contribution q_x^ρ could be of the same order of its Fourier or thermal contribution q_x^T (since $c_x^T/c_x^\rho = 2/5$) if the ‘‘shear-induced’’ density gradient is comparable to (or, larger than) the temperature gradient.

By inserting Eq. (11) into Eq. (10) and using the reference heat flux as $q_R = \rho_{av} u_R^3/2$, the dimensionless form of the tangential heat flux ($q_x \rightarrow q_x/q_R$) can be written as

$$q_x = q_x^T + q_x^\rho, \quad (13)$$

where

$$q_x^T = c_x^T \left(\frac{1}{n_{av}^*} \right)^2 \left(\frac{d}{W} \right)^2 \left(\frac{1}{\rho} \frac{du_x}{dy} \right) \frac{dT}{dy}, \quad (14)$$

$$q_x^\rho = -c_x^T \left(\frac{1}{n_{av}^*} \right)^2 \left(\frac{d}{W} \right)^2 \left(\frac{T}{\rho^2} \frac{du_x}{dy} \right) \frac{d\rho}{dy}. \quad (15)$$

In the above expressions, $n_{av}^* = n_{av} d^3$ is the reduced density and we have used $y \rightarrow y/W$, $u_x \rightarrow u_x/u_R$, $T \rightarrow T/T_w$, and $\rho \rightarrow \rho/\rho_{av}$ for nondimensionalization of remaining variables.

B. Comparison with theory and the stress-driven heat flux

Without solving the complete boundary value problem for the granular Poiseuille flow that requires boundary conditions, here we restrict to verifying whether Eqs. (9) and (13)–(15) are able to reproduce the heat flux profiles in a granular gas undergoing Poiseuille flow. By plugging the simulation data on du_x/dy , dT/dy , and $d\rho/dy$ [see Figs. 5(b), 5(d) and 5(f)] into Eqs. (14) and (15), we have calculated the transverse profiles of $q_x^T(y)$ and $q_x^\rho(y)$, see Figs. 6(a) and 6(b) for $\text{Kn} = 0.05$. It is clear from Figs. 6(a) and 6(b) that while both $q_x^T(y)$ and $q_x^\rho(y)$ are of ‘‘double-well’’

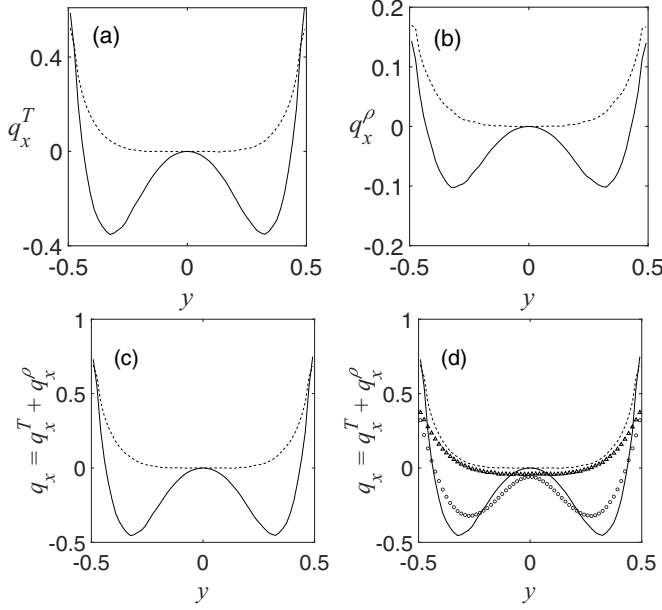


FIG. 6. Variations of (a) $q_x^T(y)$ [Eq. (14)], (b) $q_x^\rho(y)$ [Eq. (15)], and (c) $q_x^T + q_x^\rho$ [Eq. (13)] for $e_n = 1$ (dashed line) and $e_n = 0.9$ (solid line) at $\text{Kn} = 0.05$. Panel (d) is the same as panel (c), except that the DSMC data for q_x , marked by triangles ($e_n = 1$) and circles ($e_n = 0.9$), are superimposed in panel (d).

shape at $e_n = 0.9$, they are of unimodal shape in a molecular gas ($e_n = 1$); the former profiles look qualitatively similar to those in Fig. 2(a). Comparing Figs. 6(a) and 6(b), we find that the Dufour-contribution to the tangential heat flux (q_x^ρ) is comparable to its Fourier contribution (q_x^T) in a dissipative or granular gas for the specified parameter set.

Figure 6(c) displays the transverse profiles of $(q_x^T + q_x^\rho)$ and its comparison with the DSMC data is shown in Fig. 6(d). The agreement between theory and simulation is only qualitative for both $e_n = 1$ and 0.9; there are quantitative differences in the bulk of the channel (around the channel centerline where the rarefaction effects are likely to be small at $\text{Kn} = 0.05$) even for a molecular gas ($e_n = 1$). For example, the theoretical predictions of Eqs. (14) and (15) yield $q_x^T = 0 = q_x^\rho$ at the channel centerline ($y = 0$), irrespective of the value of (e_n, Kn), whereas the simulation data in Fig. 6(d) confirm $q_x(y = 0) < 0$. The latter discrepancy can partly be resolved if we consider stress-driven heat flux as demonstrated below.

A more general form of Eq. (9) can be derived from the Boltzmann equation [24,25,29] in which the heat flux is also driven by the gradients in the deviatoric stress that have been omitted in Eq. (9). The leading-order expression for the deviatoric-stress-driven tangential heat flux is taken from Reddy and Alam [29]:

$$q_x^S = -\frac{\tau_r}{\alpha(e_n)} \frac{T}{m} \left(1 - \frac{\sigma_{xx}}{nT}\right) \frac{d\sigma_{xy}}{dy} \propto \frac{d\sigma_{xy}}{dy} \sim O(\dot{\gamma}^2), \quad (16)$$

that includes all terms up to second order in gradients, same as in its Fourier [q_x^T , Eq. (14)] and Dufour [q_x^ρ , Eq. (15)] contributions; note that there are additional terms in Eq. (16) that depend on the deviatoric normal stresses (σ_{ii}) but they are of higher order in gradients and hence neglected. The dimensionless form of Eq. (16) is given by

$$q_x^S \rightarrow q_x^S/q_R = -\frac{15}{\sqrt{2\pi}(1+e_n)(49-33e_n)} \left(\frac{1}{n_{av}^*}\right) \left(\frac{d}{W}\right) \left(\frac{\sqrt{T}}{\rho}\right) \left(1 - \frac{2\sigma_{xx}}{nT}\right) \frac{d\sigma_{xy}}{dy}, \quad (17)$$

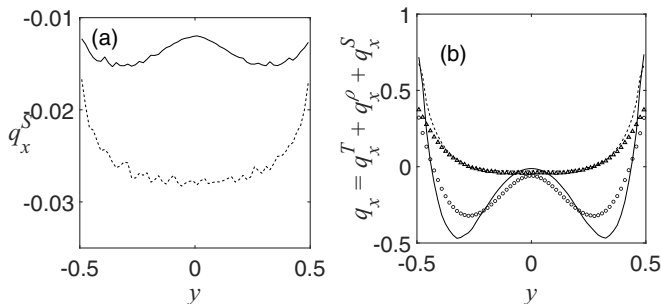


FIG. 7. Variations of (a) $q_x^S(y)$ [Eq. (17)] and (b) total $q_x^T + q_x^rho + q_x^S$ [Eq. (13)] for $e_n = 1$ (dashed line) and $e_n = 0.9$ (solid line) at $\text{Kn} = 0.05$. The DSMC data for q_x , marked by triangles ($e_n = 1$) and circles ($e_n = 0.9$), are superimposed in panel (b). The “wiggles” on curves in panel (a) are due to the calculation of derivatives (see Fig. 6(b) in Ref. [33]) from the “discrete” DSMC data.

in which we have used $\sigma_{ij} \rightarrow \sigma_{ij}/\rho_{\text{av}}u_R^2$ for dimensionless deviatoric stress (see Sec. II C in Ref. [33]), with $\sigma_{ij} = p_{ij} - p\delta_{ij}$ and $p = p_{ii}/3$. The variations of the shear stress σ_{xy} , its derivative $d\sigma_{xy}/dy$ and the deviatoric normal stress can be found in the Supplemental Material [33].

Figure 7(a) displays the transverse profiles of q_x^S [Eq. (17)] at $e_n = 1$ and 0.9, with $\text{Kn} = 0.05$. It is seen that the stress-driven tangential heat flux q_x^S is a small negative quantity for both molecular and granular gases; the magnitude of q_x^S is larger at $e_n = 1$ than that in its dissipative counterpart. The comparison of the augmented theory (including q_x^S) with the simulation data is shown in Fig. 7(b), confirming an excellent agreement between simulation and theory at $e_n = 1$ within the bulk region of the channel. In contrast, for the case of a granular gas ($e_n = 0.9$), the agreement between theory and simulation in Fig. 7(b) is only qualitative across the channel width for these parameter values.

The effect of Knudsen number on theoretical predictions can be ascertained from Figs. 8(a) and 8(b) that represent $\text{Kn} = 0.1$ and 0.025, respectively. Comparing the q_x profiles for $e_n = 1$ in Figs. 7(b), 8(a), and 8(b), we find that the disagreement between theory and simulation is confined near two walls which is due to the presence of the “Knudsen-layer” [8,9]; the width of the Knudsen-layer increases with increasing Kn . For the granular case, it is clear from Figs. 7(b), 8(a), and 8(b) that the theory can indeed capture the q_x profile quantitatively near the channel centerline at $e_n = 0.9$ if the Knudsen number is sufficiently small [$\text{Kn} = 0.025$, Figs. 8(b)]; however, the quantitative disagreement (even in the bulk of the channel) increases with increasing Kn . In particular, Fig. 8(b) indicates that while the bulk profiles of q_x remain unaffected in a mildly rarefied ($\text{Kn} = 0.025$) molecular gas ($e_n = 1$), the “wall effects” seem to be invading the bulk region of the heat-flux profiles for the dissipative case ($e_n = 0.9$). To gain more insight on observed discrepancies in Fig. 7(b) and Figs. 8(a) and 8(b), it is desirable to solve the extended set of differential equations [29] for steady, fully developed, granular Poiseuille flow with appropriate boundary conditions. In

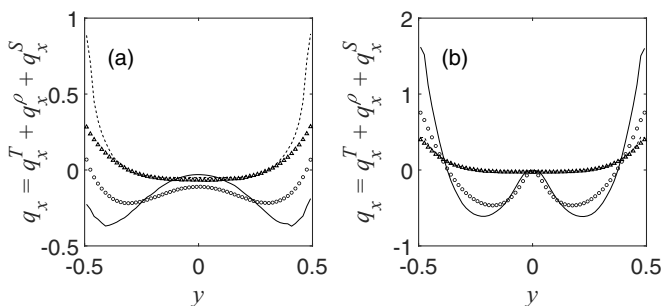


FIG. 8. Analog of Fig. 7(b) for different Knudsen numbers: (a) $\text{Kn} = 0.1$ and (a) $\text{Kn} = 0.025$.

addition to identifying the range of validity of the higher-order theory [29] in terms of (Kn, e_n) , the above exercise is likely to shed light on the importance of the Knudsen layer in granular Poiseuille flow. These issues can be resolved in a future work.

On the whole, the above analysis suggests that the deviatoric-stress-driven heat flux, though of smaller magnitude compared to (q^T, q^ρ) , should be incorporated in a generalized Fourier's law,

$$\mathbf{q} = -\kappa^T \cdot \nabla T - \kappa^\rho \cdot \nabla \rho - \kappa^S : \nabla \sigma \equiv \mathbf{q}^T + \mathbf{q}^\rho + \mathbf{q}^S, \quad (18)$$

so as to obtain quantitative prediction of the heat flux for a rarefied molecular gas undergoing Poiseuille flow. For a granular gas, however, the first two terms are dominant and the magnitude of \mathbf{q}^S decreases with increasing inelasticity. Note that Eq. (18) contains all terms that are second order in the gradients of hydrodynamic fields. Notwithstanding the quantitative differences in Fig. 7(b) and Figs. 8(a) and 8(b) for the dissipative case, we wish to emphasize that the anomalous shape of q_x profiles in GPF, that appears in the continuum limit ($\text{Kn} \rightarrow 0$), can be explained only if the cross-conductivity terms ($\kappa_{xy} \neq 0$) are incorporated, thus revealing the limitations of the ‘‘isotropic’’ Fourier's law ($\kappa_{ij} = \kappa \delta_{ij}$) for a granular gas at $\text{Kn} \sim 0$ even in the limit of nearly elastic collisions.

V. CONCLUSIONS

For the gravity-driven Poiseuille flow with isothermal walls, we found that the shear-induced heat-flux profiles and the tangential heat-flow rate in a granular gas are qualitatively different than those in a molecular gas even in the ‘‘nonrarefied’’ limit of zero Knudsen number ($\text{Kn} \rightarrow 0$). The tangential heat flux can become an order-one quantity even in a nearly elastic (e.g., $e_n = 0.9$) granular gas, signaling the failure of the isotropic Fourier's law at $\text{Kn} \rightarrow 0$.

While a generalized Fourier's law, Eq. (1), is known to correctly describe the anisotropic nature of heat transport in a rarefied ($0.1 < \text{Kn} < 10$) molecular gas, we demonstrated convincingly that a correct description of the heat transport in a nonrarefied ($\text{Kn} \rightarrow 0$) granular gas would also require a tensorial thermal conductivity, along with (i) a density-gradient driven Dufour flux term [Eq. (15)] and (ii) a deviatoric-stress-gradient driven heat flux [Eq. (17)], to be applicable over a wide range of control parameters. The validity of the linear Navier-Stokes-Fourier (NSF) model is therefore restricted to an arbitrarily small range of $(\text{Kn}, 1 - e_n) \sim (0, 0)$. Our results point toward the need for nonlinear constitutive relations for both the stress tensor [24,34–37] and the heat flux vector [29,36,38], even in the limit of zero Knudsen number of a dilute granular gas.

ACKNOWLEDGMENTS

The work of MA is partially funded by the Department of Science and Technology, Government of India, under an India-Netherlands Project (DST/INT/NL/P-03/2016).

R.G. carried out original simulations that were validated later by SR using another version of the DSMC code; Figs. 6–8 were prepared by SR during revision. The manuscript, along with the analysis in Sec. IV, was prepared by M.A..

APPENDIX: NAVIER-STOKES-FOURIER EQUATIONS AND THE GRAVITY-DRIVEN POISEUILLE FLOW

The Navier-Stokes-Fourier equations for a compressible gas are given by:

$$\left(\frac{\partial}{\partial t} + \mathbf{u} \cdot \nabla \right) \rho = -\rho \nabla \cdot \mathbf{u}, \quad (\text{A1a})$$

$$\rho \left(\frac{\partial}{\partial t} + \mathbf{u} \cdot \nabla \right) \mathbf{u} = -\nabla p - \nabla \cdot \sigma + \rho \mathbf{g}, \quad (\text{A1b})$$

$$\rho c_p \left(\frac{\partial}{\partial t} + \mathbf{u} \cdot \nabla \right) T = -\nabla \cdot \mathbf{q} - p(\nabla \cdot \mathbf{u}) - \sigma : \nabla \mathbf{u} \quad (\text{A1c})$$

that represent the conservation equations for the mass, momentum, and energy, respectively. Here $\mathbf{g} = (g, 0, 0)$ is gravitational acceleration [directed along the streamwise direction, see Fig. 1(a)], p is the pressure, $\boldsymbol{\sigma} = -\mu[\nabla\mathbf{u} + (\nabla\mathbf{u})^\dagger]$ is the deviatoric stress tensor and $\mathbf{q} = -\kappa\nabla T$ is the heat-flux vector; μ and κ represent the shear viscosity and thermal conductivity of a dilute gas.

Referring to Fig. 1(a) for the steady [$\partial/\partial t(\cdot) = 0$], fully developed [$\partial/\partial x(\cdot) = 0 = \partial/\partial z(\cdot)$ and $\partial/\partial y(\cdot) \neq 0$] plane Poiseuille flow, $\mathbf{u} = (u_x, 0, 0)$, driven by gravity, the mass balance equation and the z -momentum equation are identically satisfied. The y -momentum balance simplifies to

$$\frac{dp}{dy} = 0 \Rightarrow p(y) = \text{const} = p_0, \quad \text{and} \quad \frac{dT}{dy} = -\frac{T}{\rho} \frac{d\rho}{dy}, \quad (\text{A2})$$

with the last expression coming from the equation of state $p = \rho T$. The x -momentum balance yields

$$\frac{d\sigma_{xy}}{dy} = \rho g \Rightarrow \sigma_{xy} = \rho g y, \quad (\text{A3})$$

where σ_{xy} is the shear stress that varies linearly with the wall-normal coordinate y , as verified in Fig. 6(a) in the Supplemental Material [33].

Equation (A3) can be rewritten as

$$\frac{du_x}{dy} = -\frac{\rho g}{\mu} y \equiv \dot{\gamma}(y), \quad (\text{A4})$$

and therefore, the local shear rate [see its variation with y in Fig. 5(f)] is proportional to the gravitational acceleration and inversely proportional to the shear viscosity. The parabolic shape of the velocity profile $u_x(y)$ is evident from Eq. (A4) if the shear viscosity and the density are assumed to be constant which is, of course, not applicable for a compressible gas. The energy balance equation simplifies to

$$\frac{dq_y}{dy} + \sigma_{xy} \frac{du_x}{dy} = 0 = \frac{d}{dy} \left(\kappa \frac{dT}{dy} \right) + \mu \left(\frac{du_x}{dy} \right)^2, \quad (\text{A5})$$

where the last expression follows from the Fourier's law of heat flux and the Newton's law of viscosity. Because of the temperature dependence of both $\mu(T) \propto T^\alpha$ and $\kappa(T) \propto T^\alpha$ (with $\alpha = 1$ and $1/2$ for Maxwell molecules and a hard-sphere gas, respectively), the closed-form analytical solution of (A4) and (A5) does not seem possible. However, some progress can be made if the strength of the gravitational acceleration \hat{g} , Eq. (3), is assumed to be small and the analysis is carried out around the channel centerline [6].

Referring to Figs. 5(a)–5(d), we note that the density and temperature profiles (see the dashed lines for a molecular gas with $\text{Kn} = 0.05$) are nearly flat (with negligible gradients) around the channel centerline $y = 0$. Therefore, as a first approximation, (μ, κ, ρ, T) in Eqs. (A4)–(A5) are replaced by their values $(\mu_0, \kappa_0, \rho_0, T_0)$ at $y = 0$. The solutions to the resulting Eqs. (A4)–(A5) yield the velocity and temperature profiles as

$$u_x(y) = u(0) - \frac{\rho_0 g}{\mu_0} y^2, \quad (\text{A6})$$

$$T(y) = T(0) - \frac{\rho_0^2 g^2}{12\mu_0\kappa_0} y^4. \quad (\text{A7})$$

Note that the odd-order terms in g contribute to the velocity profile, while the even-order terms in g contribute to the temperature profile. The expression for the density profile follows from Eq. (A2):

$$\rho(y) = \rho_0 \left[T(0) - \frac{\rho_0^2 g^2}{12\mu_0\kappa_0} y^4 \right]^{-1}. \quad (\text{A8})$$

Therefore, the gravity-driven Poiseuille flow does admit steady, streamwise-independent profiles of hydrodynamic fields [6–10].

- [1] J. C. Maxwell, On stresses in rarefied gases arising from inequalities of temperature, *Phillos. Trans. R. Soc. Lond.* **170**, 231 (1879).
- [2] M. Knudsen, Die Gesetze der Molekularströmung und der inneren Reibungsströmung der Gase durch Röhren, *Ann. Phys.* **333**, 75 (1909).
- [3] D. Burnett, The distribution velocities in a slightly non-uniform gas, *Proc. Lond. Math. Soc.* **s2-39**, 385 (1935).
- [4] H. Grad, On the kinetic theory of rarefied gases, *Commun. Pure Appl. Maths.* **2**, 331 (1949).
- [5] C. Cercignani and A. Daneri, Flow of a rarefied gas between two parallel plates, *J. Appl. Phys.* **34**, 3509 (1963).
- [6] M. Tij and A. Santos, Perturbation analysis of a stationary non-equilibrium flow generated by external force, *J. Stat. Phys.* **76**, 1399 (1994).
- [7] M. M. Mansour, F. Baras, and A. L. Garcia, On the validity of hydrodynamics in plane Poiseuille flows, *Physica A* **240**, 255 (1999).
- [8] F. J. Uribe and A. L. Garcia, Burnett description for plane Poiseuille flow, *Phys. Rev. E* **60**, 4063 (1999).
- [9] K. Aoki, S. Takata, and T. Nakanishi, Poiseuille-type flow of a rarefied gas between two parallel plates driven by a uniform external force, *Phys. Rev. E* **65**, 026315 (2002).
- [10] R. Rongali and M. Alam, Asymptotic expansion and Padé approximants for acceleration-driven Poiseuille flow of a rarefied gas: Bulk hydrodynamics and rheology, *Phys. Rev. E* **98**, 012115 (2018).
- [11] Z. Ding, J. Zhou, B. Song, V. Chiloyan, M. Li, T.-H. Liu, and G. Chen, Phonon hydrodynamic heat conduction and Knudsen minimum in graphite, *Nano Lett.* **18**, 638 (2018).
- [12] J. T. Jenkins and S. B. Savage, A theory for the rapid flow of identical, smooth, nearly elastic, spherical particles, *J. Fluid Mech.* **130**, 187 (1983).
- [13] R. Jackson, *Dynamics of Fluidized Particles* (Cambridge University Press, Cambridge, 2000).
- [14] T. Pöschel and S. Luding, *Granular Gases* (Springer, Berlin, 2001).
- [15] I. Goldhirsch, Rapid granular flows, *Annu. Rev. Fluid Mech.* **35**, 267 (2003).
- [16] M. Alam, A. Mahajan, and D. Shivanna, On Knudsen-minimum effect and temperature-bimodality in dilute granular Poiseuille flow, *J. Fluid Mech.* **782**, 99 (2015).
- [17] R. Gupta and M. Alam, Hydrodynamics, wall-slip, and normal-stress differences in rarefied granular Poiseuille flow, *Phys. Rev. E* **95**, 022903 (2017).
- [18] R. Gupta and M. Alam, Disentangling the role of athermal walls on the Knudsen paradox in molecular and granular gases, *Phys. Rev. E* **97**, 012912 (2018).
- [19] M. Tij and A. Santos, Poiseuille flow in a heated granular gas, *J. Stat. Phys.* **117**, 901 (2004).
- [20] R. Rongali and M. Alam, Asymptotic expansion and Padé approximants for gravity-driven flow of a heated granular gas: Competition between inelasticity and forcing, up-to Burnett order, *Phys. Rev. E* **98**, 052144 (2018).
- [21] B. D. Todd, P. J. Daivis, and D. J. Evans, Heat flux vector in highly inhomogeneous non-equilibrium fluids, *Phys. Rev. E* **51**, 4362 (1995).
- [22] P. J. Daivis and J. L. K. Coelho, Generalized Fourier law for heat flow in a fluid with a strong, non-uniform strain rate, *Phys. Rev. E* **61**, 6003 (2000).
- [23] V. Garzo, Heat flux induced by an external force in a strongly dilute gas, *J. Chem. Phys.* **101**, 1423 (1994).
- [24] S. Saha and M. Alam, Non-Newtonian stress, collisional dissipation and heat flux in the shear flow of inelastic disks: A reduction via Grad's moment method, *J. Fluid Mech.* **757**, 251 (2014).
- [25] M. Alam and S. Saha, Normal stress differences and beyond-Navier-Stokes hydrodynamics, *EPJ Web Conf.* **140**, 11014 (2017).
- [26] C. F. Curtiss and R. B. Bird, Statistical mechanics of transport phenomena: Polymeric liquid mixtures, *Adv. Polym. Sci.* **125**, 1 (1996).
- [27] D. C. Venerus, J. D. Schieber, V. Balasubramanian, K. Bush, and S. Smoukov, Anisotropic Thermal Conduction in a Polymer Liquid Subjected to Shear Flow, *Phys. Rev. Lett.* **93**, 098301 (2004).
- [28] H. C. Öttinger, Relativistic and non-relativistic description of fluids with anisotropic heat conduction, *Physica A* **254**, 433 (1998).
- [29] M. H. L. Reddy and M. Alam, Regularized extended hydrodynamic equations for a rarefied granular gas and the plane shock waves, *Phys. Rev. Fluids* **5**, 044302 (2020).

- [30] M. N. Kogan, *Rarefied Gas Dynamics* (Plenum Press, New York, 1969).
- [31] G. A. Bird, *Molecular Gas Dynamics and the Direct Simulation Monte Carlo of Gas Flows* (Clarendon, Oxford, 1994).
- [32] T. Pöschel and T. Schwager, *Computational Granular Dynamics* (Springer, Berlin, 2005).
- [33] See Supplemental Material at <http://link.aps.org/supplemental/10.1103/PhysRevFluids.6.114303> for (i) a description of the simulation method and (ii) the profiles of hydrodynamic fields and (iii) the related auxiliary data on heat flux.
- [34] S. Saha and M. Alam, Normal stress differences, their origin and constitutive relations for a sheared granular fluid, *J. Fluid Mech.* **795**, 549 (2016).
- [35] J. T. Jenkins and M. W. Richman, Grad's 13-moment for a dense gas of inelastic spheres, *Arch. Ration. Mech. Anal.* **87**, 355 (1985).
- [36] N. Sela and I. Goldhirsch, Hydrodynamic equations for rapid flows of smooth inelastic spheres, upto Burnett order, *J. Fluid Mech.* **361**, 41 (1998).
- [37] J. T. Jenkins, M. Alam, and D. Berzi, Singular behaviour of the stresses in the limit of random close packing in collisional, simple shearing flows of frictional spheres, *Phys. Rev. Fluids* **5**, 072301(R) (2020).
- [38] M. Alam and S. Saha, Generalized Fourier's law and the anisotropic conductivity tensors in a sheared granular gas (unpublished).